In solution, the (η^5-pd)FeL_3^+ complexes undergo dynamic processes involving rotation of the pd ligand with respect to the FeL_3 fragment.

Currently, we are attempting to functionalize the decatetraene ligands in **5** and **6** and are probing the reactivity of cationic complexes **7**, **8**, and **9** toward nucleophiles. Results of these studies will be reported in the future.

Acknowledgment. Support from the National Science Foundation (Grant CHE-8520680) is gratefully acknowledged. Washington University's High Resolution NMR Service Facility was funded in part by National Institutes of Health Biomedical Research Support Instrument Grant 1 S10 RR02004 and by a gift from Monsanto Company. M.K.H. thanks the AAUW Educational Foundation for providing a Dissertation Fellowship. We thank Patricia Earl for synthesizing $(Me_2PCH_2)_3CMe$.

Registry No. **1**, 88765-93-9; **2**, 113948-15-5; **3**, 113975-07-8; **4**, 113948-16-6; **5**, 113975-08-9; **6**, 113948-17-7; **7a**, 113948-19-9; **7b**, 114029-28-6; **8a**, 113948-21-3; **8b**, 114029-27-5; **9a** (isomer A), 114029-31-1; **9a** (isomer B), 114127-19-4; **9b** (isomer A), 113948-24-6; **9b** (isomer B), 114029-30-0; K^+Pd^-, 51391-25-4; $FeCl_2(PEt_3)_2$, 95075-11-9; $FeCl_2(P(n\text{-}Pr)_3)_2$, 113948-22-4; PMe_3, 594-09-2; $(Me_2PCH_2)_3CMe$, 77609-83-7; $P(OMe)_3$, 121-45-9.

Supplementary Material Available: Listings of final atomic coordinates, thermal parameters, bond lengths, bond angles, and significant least-squares planes for **3**, **5**, and **7a** (19 pages); listings of observed and calculated structure factor amplitudes for **3**, **5**, and **7a** (36 pages). Ordering information is given on any current masthead page.

Electronic Structures and EPR Spectra of Carbonylbis(cyclopentadienyl)vanadium(II) and Carbonylbis(pentadienyl)vanadium(II)

Ruth M. Kowaleski,† Fred Basolo,† Joseph H. Osborne,‡ and William C. Trogler*,‡

Department of Chemistry, Northwestern University, Evanston, Illinois 60201, and Department of Chemistry, D-006, University of California at San Diego, La Jolla, California 92093

Received December 22, 1987

The electronic structures of Cp_2V and pd_2V, where Cp = η-C_5H_5 and pd = η-C_5H_7, have been modeled by spin-restricted and spin-polarized SCF–Xα–DV calculations. In agreement with the experimental magnetic moments Cp_2V is calculated to adopt a high spin (three unpaired electrons) ground electronic state and pd_2V contains one unpaired electron. While the d orbitals in Cp_2V split in a pseudooctahedral pattern those in pd_2V show a considerable distortion and splitting. Calculations for the carbonyl adducts Cp_2VCO and pd_2VCO show the highest occupied orbital is $12a_1$ in both cases, which yields a $^2A_1$ ground state. The vanadium atom is calculated to be more positively charged in the pd derivative and this conforms to the 80 cm^{-1} higher IR CO stretching frequency in this complex. Radical reactivity depends critically on the $12a_1$ orbital. In Cp_2VCO orbital contour plots show the odd electron in a a_1 d orbital hybrid localized between the two cyclopentadienyl ring planes; however, in pd_2VCO the $12a_1$ orbital is calculated to point toward the center of the pd ligands. The EPR spectra of the complexes pd_2VCO, pd'_2VCO, Cp(pd)VCO, Cp(pd')VCO, Cp_2VCO, and Cp^*_2VCO (where Cp* = η-$C_5(CH_3)_5$ and pd' = 2,4-$(CH_3)_2C_5H_5$) and their ^{13}CO derivatives at room temperature and in frozen methylcyclohexane are reported. The isotropic coupling constants for this series of complexes range from -7.36×10^{-3} cm^{-1} (79.1 G) for pd_2VCO to -1.73×10^{-3} cm^{-1} (18.6 G) for Cp^*_2VCO. The EPR parameters indicate greater covalency and lower charge on vanadium in the cyclopentadienyl complexes as compared to the pentadienyl complexes and support the conclusions of the SCF–Xα–DV calculations. Small hyperfine splittings from delocalization of the unpaired electron onto the CO ligand were observed for $Cp_2V^{13}CO$ and $Cp^*_2V^{13}CO$ (A^C_{iso} = 9.3×10^{-4} and 10.7×10^{-4} cm^{-1}, respectively). No evidence for delocalization onto the CO ligand could be found in the complexes containing pentadienyl ligands.

Introduction

Electronic structures of 17-electron complexes might contain information to help one understand the enhanced reactivity of these complexes as compared to their 18-electron analogues. Studies of 17-electron metal carbonyl complexes such as $V(CO)_6$, $Mn(CO)_5$, $Fe(CO)_3(PR_3)_2^+$, and $(\eta^4$-$C_4H_6)_2MnCO$ suggest the extent of delocalization of the unpaired electron onto the ligands and the directional properties of the singly occupied molecular orbital (SOMO) may help to explain the associative substitution lability of these complexes.[1-5] One thesis we have favored[5] is stabilization of 19-electron transition states or intermediates by bonding between a pair of electrons on an attacking nucleophile and an orbital on the metal that is half-occupied in the radical.

The 17-electron vanadocene derivatives (η^5-L)$_2$VCO (η^5-L = Cp = C_5H_5, Cp* = C_5Me_5, pd' = 2,4-$Me_2C_5H_5$, and

† Northwestern University.
‡ University of California at San Diego.

(1) Bratt, S. W.; Kassyk, A.; Perutz, R. N.; Symons, M. C. R. *J. Am. Chem. Soc.* **1982**, *104*, 490–494.
(2) (a) McCall, J. M.; Morton, J. R.; Preston, K. F. *J. Magn. Reson.* **1984**, *64*, 414–419. (b) Howard, J. A.; Morton, J. R.; Preston, K. F. *Chem. Phys. Lett.* **1981**, *83*, 226–228.
(3) Herrinton, T. R.; Brown, T. L. *J. Am. Chem. Soc.* **1985**, *107*, 5700–5703.
(4) Harlow, R. L.; Krusic, P. J.; McKinney, R. J.; Wreford, S. S. *Organometallics* **1982**, *1*, 1506–1513.
(5) (a) Holland, G. F.; Manning, M. C.; Ellis, D. E.; Trogler, W. C. *J. Am. Chem. Soc.* **1983**, *105*, 2308–2314. (b) Shi, Q.-Z.; Richmond, T. G.; Trogler, W. C.; Basolo, F. *Ibid.* **1982**, *104*, 4032–4034; **1984**, *106*, 71–76. (c) Therien, M. J.; Trogler, W. C. *Ibid.* **1986**, *108*, 3697–3702. (d) Therien, M. J.; Ni, C. L.; Anson, F. C.; Osteryoung, J. G.; Trogler, W. C. *Ibid.* **1986**, *108*, 4037–4042. (e) Trogler, W. C. *Int. J. Chem. Kinet.* **1987**, *19*, 1025–1047.

0276-7333/88/2307-1425$01.50/0

pd = C_5H_7) show significant differences in their IR carbonyl stretching frequencies (ν_{CO} = 1842 cm^{-1} for Cp^*_2VCO and 1959 cm^{-1} for pd_2VCO) as well as in their reactivities. Thus, replacement of a cyclopentadienyl ligand with pentadienyl may have a considerable effect on the electronic structure of these complexes. The five π molecular orbitals of the U-shaped pentadienyl moiety can interact with metal orbitals as does Cp, although the differing energies of the ligand orbitals may lead to different ground-state configurations.[6-8] For example, the ground state for the 15-electron complex pd'_2V contains one unpaied electron,[8] while Cp_2V and Cp^*_2V contain three unpaired electrons.[9] Vanadium–pentadienyl bonding also appears stronger than vanadium–cyclopentadienyl bonding in analogous complexes.[6] Pentadienyl ligands have attracted interest as open analogues of the cyclopentadienyl ligand that may impart enhanced reactivity to metal centers. In understanding the comparative chemistry of pd and Cp complexes one must understand differences or similarities in their orbital interactions with metals. Our interest in reaction mechanisms of organometallic radicals led us to examine the lability of CO in Cp_2VCO and pd_2VCO. The unexpected finding[10] that the rate for associative substitution of CO in pd_2VCO was 10^{-5} that of Cp_2VCO suggests a difference in electronic structures for these complexes. Herein we report SCF–DV–Xα calculations and detailed EPR spectroscopic studies to define the bonding in bis(cyclopentadienyl) and bis(pentadienyl) complexes of vanadium(II).

Experimental Section

EPR Spectra. Solutions of the vanadium carbonyl complexes[10] in methylcyclohexane (10^{-3}–10^{-4} M) under an atmosphere of N_2 or CO were prepared in 4-mm quartz tubes fitted with Teflon stopcocks. EPR spectra were recorded at X-band frequency on a Varian E-4 spectrometer and calibrated with a strong pitch standard (g = 2.0028). Spectra were obtained at ambient temperature and at liquid-nitrogen temperature using a quartz-insertion Dewar. The EPR spectra were simulated by using a version of the QPOW EPR simulation program.[11] Room-temperature spectra were fit by using Lorentzian line shapes, and Gaussian line shapes were used to simulate frozen solution spectra.

Calculations. Electronic structure calculations were performed with a DEC-VAX 11/780 minicomputer and used the self-consistent field discrete variational Xα (SCF–DV–Xα) method.[12] Numerical atomic orbitals from exact Hartree–Fock–Slater calculations were used as basis functions, assuming the α values of Schwartz.[13] For V, the atomic orbitals through 4p were included. For C a minimal (1s, 2s, and 2p) basis was used. For H, a 1s function was used. Core orbitals (1s, ..., 3p for V and 1s for C and O) were frozen and orthogonalized against valence orbitals.

Table I. SCF-Xα-DV Calculations for Vanadocene

level[a]	energy (eV)	% contributns from atoms V	C	H
$1e_{2u}$	−1.56	0	99	1
$2e_{1g}$	−3.68	54	46	0
$2a_{1g}$	−5.86	87	12	1
$1e_{2g}$	−6.11	89	10	1
$1e_{1u}$	−8.74	0	100	0
$1e_{1g}$	−9.44	23	76	0
$1a_{2u}$	−11.91	0	100	0
$1a_{1g}$	−12.60	2	90	8

[a] Highest occupied molecular orbital is $1e_{2g}$ in the spin-restricted calculation; however, $2a_{1g}$ is occupied in the spin-polarized results.

Table II. SCF-Xα-DV Calculations for Bis(pentadienyl)vanadium

level[a]	energy (eV)	% contributns from atoms[b] V	C1	C2	C3	H
18b	−1.42	2	26	42	29	1
19a	−1.58	6	23	35	35	2
18a	−2.60	33	33	30	3	1
17b	−3.42	36	38	12	11	2
16b	−3.91	26	28	36	7	3
17a	−3.98	49	16	15	16	4
15b	−5.32	67	26	3	2	1
16a	−5.78	77	11	5	2	6
15a	−6.67	57	25	12	1	4
14a	−7.73	14	50	2	30	3
14b	−8.37	31	43	3	22	1
13b	−10.02	5	43	51	0	1
13a	−10.02	4	40	54	1	1

[a] Highest occupied molecular orbital is 16a. [b] C1 = terminal α-carbon atoms. C2 = β-carbon atoms. C3 = unique γ-carbon atom. All hydrogens were treated as a single potential type.

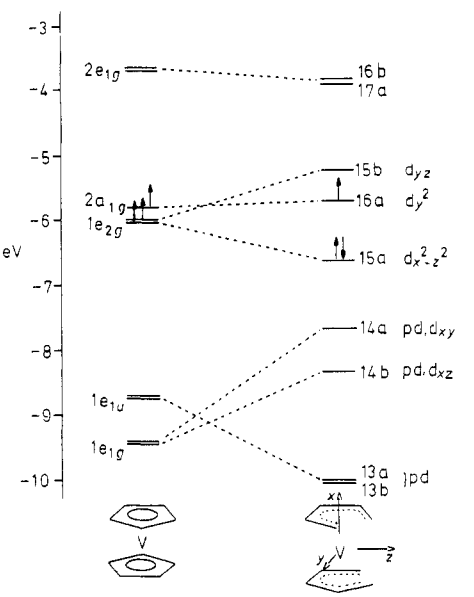

Figure 1. Results of SCF–DV–Xα calculations for Cp_2V and pd_2V. For Cp_2V the z axis was taken coincident with the molecular C_5 axis, and for pd_2V the coordinate system used is defined in the figure.

The Mulliken[14] scheme was used to compute atomic orbital populations. The molecular Coulomb potential was calculated by using a least-squares fit[15] of the model electron density to the true density. Seven radial degrees of freedom were included in the expansion of the density, in addition to the radial atomic

(6) (a) Ernst, R. D. *Acc. Chem. Res.* **1985**, *18*, 56–62. (b) Ernst, R. D. *Struct. Bonding (Berlin)* **1984**, *57*, 1–53.
(7) Böhm, M. C.; Eckert-Maksic, M.; Ernst, R. D.; Wilson, D. R.; Gleiter, R. *J. Am. Chem. Soc.* **1982**, *104*, 2699–2707.
(8) Ernst, R. D.; Campana, C. F.; Wilson, D. R.; Liu, J.-Z. *Inorg. Chem.* **1984**, *23*, 2732–2734.
(9) (a) Prins, R.; Van Voorst, J. D. W. *J. Chem. Phys.* **1968**, *49*, 4665–4673. (b) Ammeter, J. H. *J. Magn. Reson.* **1978**, *30*, 299–325. (c) Robbins, J. L.; Edelstein, N.; Spencer, B.; Smart, J. C. *J. Am. Chem. Soc.* **1982**, *104*, 1882–1893.
(10) (a) Kowaleski, R. M.; Trogler, W. C.; Basolo, F. *Gazz. Chim. Ital.* **1986**, *116*, 105–107. (b) Kowaleski, R. M.; Basolo, F.; Trogler, W. C.; Ernst, R. D. *J. Am. Chem. Soc.* **1986**, *108*, 6046–6048. (c) Kowaleski, R. M.; Basolo, F.; Trogler, W. C.; Gedridge, R. W.; Newbound, T. D.; Ernst, R. D. *J. Am. Chem. Soc.* **1987**, *109*, 4860–4869.
(11) The XPOW version of the QPOW program as modified by J. Telser was used. QPOW EPR Simulation Program c 1980 by R. L. Belford and co-workers: (a) Liczwek, D. L.; Belford, R. L.; Pilbrow, J. R.; Hyde, J. S. *J. Chem. Phys.* **1983**, *87*, 2509–2512. (b) Nilges, M. J. Ph.D. Thesis, University of Illinois, 1981. Altman, T. E. *Ibid.* 1981. Maurice, A. M. *Ibid.* **1983**, Duliba, E. P. *Ibid.* 1983.
(12) Ellis, D. E.; Painter, G. S. *Phys. Rev. B: Solid State* **1970**, *2*, 2887–2898.
(13) Schwartz, K. *Phys. Rev. B: Solid State* **1972**, *5*, 2466.
(14) Mulliken, R. S. *J. Chem. Phys.* **1955**, *23*, 1833–1840.
(15) Delley, B.; Ellis, D. E.; Freeman, A. J.; Baerends, E. J. Post, D. *Phys. Rev. B: Condens. Matter* **1983**, *27*, 2132–2144.

Table III. Population Analyses for Cp_2V and pd_2V

$V(C_5H_5)_2$			$V(C_5H_7)_2$		
V	3d	3.48	V	3d	3.49
	4s	−0.32		4s	−0.18
	4p	0.90		4p	0.87
		+0.93[a]			+0.82[a]
C	2s	1.55	C1	2s	1.59
	2p	2.65		2p	2.75
		−0.20[a]			−0.34[a]
			C2	2s	1.56
				2p	2.54
					−0.10[a]
			C3	2s	1.45
				2p	2.75
					−0.19[a]
H	1s	0.89	H	1s	0.90
		+0.11[a]			+0.10[a]

[a] Total charge.

densities. For the molecular exchange potential we set $\alpha = 0.716$. Spin-restricted SCF–DV–Xα calculations were performed to deduce qualitative bonding features. Spin-polarized SCF–DV–Xα calculations were used to determine the spin state and spin distribution.

Structural models for vanadocene and vanadocene carbonyl were taken from published structures.[16a–c] Vanadocene carbonyl was calculated in C_{2v} symmetry. The model for bis(pentadienyl)vanadium and bis(pentadienyl)vanadium carbonyl were adapted to C_2 and C_{2v} symmetry from the published structure[16d] and from structures of titanium phosphine analogues,[6b] respectively. For pd_2VCO the pentadienyl rings were eclipsed and set parallel to one another. A calculation for pd_2VCO, where the pd rings were bent back (15°) similar to the Cp_2VCO structure, did not show major changes in the orbital energy scheme. The V–C–O distances were assumed equal to those in the decamethyl vanadocene structure.[16c]

Results and Discussion

Calculations for Vanadocene and for Bis(pentadienyl)vanadium. Results of calculations in spin-restricted form for Cp_2V ($S = {}^1/_2$) and for pd_2V are given in Tables I and II, with Figure 1 comparing the orbital energies. For vanadocene the principal V–Cp bonding orbital is $1e_{1g}$ and the orbital level scheme is the same as proposed[17] for other metallocenes of first-row transition metals. The vanadium atom sits in a pseudooctahedral environment with $10Dq$ being ~2.34 eV. The "t_{2g}"-derived orbitals ($1e_{2g}$ and $2a_{1g}$) lie within 0.3 eV of each other. Three unpaired electrons must occupy both orbitals to be consistent with the observed magnetic moment[9] of 3.78 μ_β. A spin-restricted calculation with $S = {}^3/_2$ resulted in a slight shift of all levels downward by about 0.05 eV with no change in the charge distribution for any atom or orbital. Although transition-state calculations were not performed, the $2e_{1g}$–$2a_{1g}$ (Δ_1 = 2.18 eV) and $2a_{1g}$–$1e_{2g}$ (Δ_2 = 0.25 eV) separations compare well with the values of Δ_1 = 2.0–2.1 eV and Δ_2 = 0.5–0.6 eV determined by optical spectroscopy.[17]

For pd_2V the low C_2 symmetry allows extensive mixing of atomic orbitals. This hinders a qualitative assignment of the molecular orbitals. The 14a and 14b orbitals contain substantial V–pd bonding character. These orbitals lie higher in energy than the corresponding orbitals in Cp_2V. This may result from the lower molecular symmetry and higher energy of the HOMO for the pentadienyl vs cyclopentadienyl ligand. Figure 1 shows that pd_2V differs from vanadocene in the energetic separations among the highest occupied molecular orbitals. Where Cp_2V has close to octahedral symmetry about vanadium, pd_2V shows considerable distortion. The orbitals 15a and 15b split by almost 1.4 eV about 16a, the highest occupied orbital. The result should be a low-spin system with one unpaired electron as found experimentally.[18] Spin-polarized calculations were also performed and predict, at a higher level of theory, the low-spin ground state for pd_2V. For both molecules we calculate the vanadium atom to be positively charged: +0.93 and +0.82 for Cp_2V and pd_2V, respectively (Table III).

Spin-polarized calculations for Cp_2V show the two highest occupied orbitals to be close in energy and spin up, which confirms the conclusions derived from the experimental magnetic moment and spin-restricted calculations. Significant shifts between the spin up and down components (i.e. an exchange splitting) occur only for metal localized orbitals. Minimal spin delocalizes (Table IV) onto the Cp ligands. A spin-polarized calculation for pd_2V shows it to be a $S = {}^1/_2$ system. The calculated spin

Table IV. Population and Spin Distribution Analyses for Spin-Polarized Calculations of Cp_2V and pd_2V

$V(C_5H_5)_2$				$V(C_5H_7)_2$			
		charge	spin			charge	spin
V	3d	3.57	+3.05	V	3d	3.49	+1.38
	4s	−0.38	+0.10		4s	−0.18	−0.01
	4p	0.90	+0.05		4p	0.87	−0.10
		+0.91[a]				+0.82[a]	
C	2s	1.55	−0.00	C1	2s	1.59	−0.00
	2p	2.65	−0.04		2p	2.75	−0.06
			−0.20[b]			−0.34[b]	
				C2	2s	1.56	+0.00
					2p	2.54	−0.00
						−0.10[b]	
				C3	2s	1.45	−0.00
					2p	2.74	−0.04
						−0.19[b]	
H	1s	0.89	+0.01	H	1s	0.91	+0.01
			+0.11[b]				+0.09[b]

[a] Total charge. [b] Total charge per atom.

Table V. Population Analyses for Spin-Polarized Calculations of Cp_2VCO and pd_2VCO

$V(C_5H_5)_2CO$				$V(C_5H_7)_2CO$			
		charge	spin			charge	spin
V	3d	3.41	+1.345	V	3d	3.53	+1.424
	4s	0.09	+0.021		4s	−0.20	−0.072
	4p	1.10	+0.001		4p	1.06	−0.200
		+0.41[a]				+0.61[a]	
C	2s	1.60	−0.019	C	2s	1.73	−0.015
	2p	2.26	−0.157		2p	2.23	−0.109
		0.14[a]				0.04[a]	
O	2s	2.00	0.006	O	2s	2.21	+0.002
	2p	4.11	−0.053		2p	3.85	−0.027
		−0.10[a]				−0.06[a]	
C_{Cp}	2s	1.53	−0.001	C_{pd}	2s	1.54	0.001
	2p	2.62	−0.022		2p	2.64	−0.034
		−0.14[b]				−0.19[b]	
H	1s	0.90	+0.005	H	1s	0.91	+0.009
		+0.1[b]				+0.09[b]	

[a] Total charge. [b] Total charge per atom.

(16) (a) Antipin, M. Yu.; Lobkovskii, E. B.; Semenenko, K. N.; Soloveichik, G. L.; Struchkov, Yu. T. *J. Struct. Chem. (Engl. Transl.)* **1979**, *20*, 810–814. (b) Gard, E.; Haaland, A.; Novak, D. P.; Seip, R. *J. Organomet. Chem.* **1975**, *88*, 181–187. (c) Gambarotta, S.; Floriani, C.; Chiesi-Villa, A.; Guastini, C. *Inorg. Chem.* **1984**, *23*, 1739–1747. (d) Ernst, R. D.; Campana, C. F.; Wilson, D. R.; Liu, J.-Z. *Inorg. Chem.* **1984**, *23*, 2732–2734.

(17) Warren, K. D. *Struct. Bonding (Berlin)* **1976**, *127*, 45–86. Green, J. C. *Ibid.* **1981**, *43*, 37–112. Modelli, A.; Foffani, A.; Guerra, M.; Jones, D.; Distefano, G. *Chem. Phys. Lett.* **1983**, *99*, 58–65.

(18) DiMauro, P. T.; Wolczanski, P. T. *Organometallics* **1987**, *6*, 1947–1954.

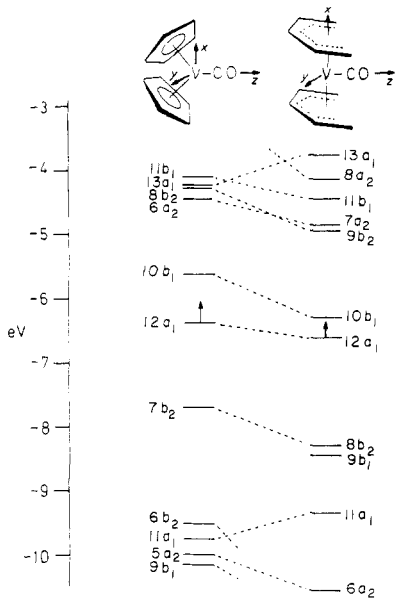

Figure 2. Results of SCF-DV-Xα calculations for Cp_2VCO and pd_2VCO. The coordinate system chosen is defined in the figure.

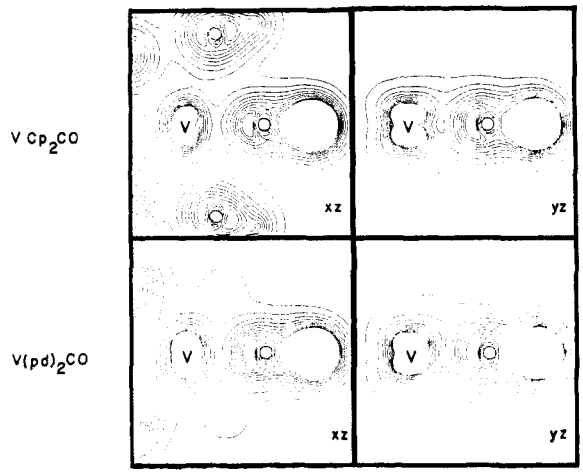

Figure 3. Total electron density plots for Cp_2VCO and pd_2VCO in the xz and yz planes. The contour interval is 0.169 $e^2/Å^3$.

distribution shown in Table IV suggests that most of the spin density localizes on the vanadium atom as was found for Cp_2V.

Calculations for Carbonyl Adducts. Calculated atomic populations and charge distributions for Cp_2VCO and pd_2VCO are shown in Table V, and the orbital energy schemes are compared in Figure 2. Consistent with Ernst's observations[6] the vanadium atom (Table V) becomes more positively charged and the diene ligand becomes more negatively charged for the pentadienyl complex. The greater calculated negative charge for CO in Cp_2VCO suggests greater M → CO back-bonding, which agrees with the lowered IR stretching frequency.

Total density plots (Figure 3) imply that V-CO σ bonding in pd_2VCO exceeds that in Cp_2VCO. The xz plane π-bonding ($9b_1$ orbital) appears weak in both complexes. The yz-plane π-bonding is slightly stronger for Cp_2VCO. Both total density plots and $7b_2$ ($8b_2$ for pd_2VCO) orbital contour maps (Figure 4) support these conclusions. The $7b_2$ ($8b_2$) orbital exhibits metal to ligand dπ–π^* back-bonding character. The observed IR stretching frequencies also suggest increased π-back bonding in Cp_2VCO (1881 cm^{-1}) vs pd_2VCO (1959 cm^{-1}). The more positive metal center in pd_2VCO should contract the vanadium d orbitals and lead to poorer overlap with the CO π^* orbitals. Charge

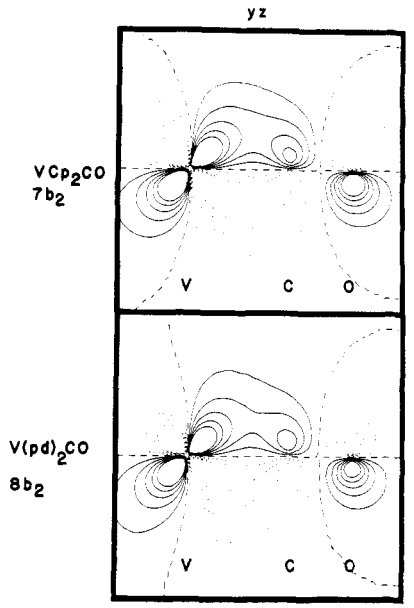

Figure 4. Orbital contour plots in the yz plane for the occupied V–CO π-bonding $7b_2$ orbital in Cp_2VCO and $8b_2$ orbital in pd_2VCO. The contour interval is 0.270 $e/Å^3$.

Table VI. SCF-Xα-DV Calculation Results for Cp_2VCO

		% contributns from atoms					
level	energy (eV)	V	C	O	Cp	metal d	bond type
$9b_2$	−2.34	17	3	1	80	yz	
$14a_1$	−2.36	18	1	1	81	$x^2 - z^2$	
$12b_1$	−2.37	1	11	6	83		
$7a_2$	−2.53	2	0	0	97		
$11b_1$	−4.10	35	25	15	25	xz	M–CO π^*
$13a_1$	−4.23	52	21	3	24	$z^2 - x^2$	M–CO σ^*
$8b_2$	−4.28	25	36	25	14	yz	M–CO π^*
$6a_2$	−4.45	54	0	0	46		
$10b_1$	−5.63	19	15	17	49	xz	M–CO π
$12a_1$	−6.39[a]	84	1	0	14	y^2	
$7b_2$	−7.70	65	14	14	7	yz	M–CO π
$6b_2$	−9.51	2	0	0	98		
$11a_1$	−9.76	10	0	0	90	$z^2 - x^2$	
$5a_2$	−9.98	21	0	0	79		
$9b_1$	−10.14	24	1	8	67	xz	
$8b_1$	−12.33	1	0	7	91		
$10a_1$	−12.51	10	15	9	66	$z^2 - x^2$	M–CO σ

[a] Denotes highest occupied orbital.

Table VII. SCF-Xα-DV Calculation Results for pd_2VCO

		% contributns from atoms					
level	energy (eV)	V	C	O	pd	metal d	bond type
$14a_1$	−2.15	11	0	0	90	$z^2 - y^2$	
$10b_2$	−3.63	34	6	2	58	yz	
$13a_1$	−3.77	49	16	5	29	z^2	M–CO σ^*
$8a_2$	−4.15	14	0	0	86		
$11b_1$	−4.44	39	20	10	31	xz	M–CO π^*
$7a_2$	−4.83	45	0	0	55	xy	
$9b_2$	−4.96	6	36	28	29		M–CO π^*
$10b_1$	−6.30	5	29	22	44		M–COπ^*
$12a_1$	−6.61[a]	79	1	0	23	x^2	
$8b_2$	−8.28	53	6	9	33	yz	M–CO π
$9b_1$	−8.46	24	1	5	70	xz	
$11a_1$	−9.36	14	1	0	85	$x^2 - y^2$	M–pd
$6a_2$	−10.57	10	0	0	90		

[a] Denotes highest occupied orbital.

distributions for the orbitals (Table VI and VII) show less covalency in pd_2VCO. For example, the lowest unoccupied orbital, $10b_1$, correlates with a CO π^* orbital bound to the metal d_{xz} orbital (Figure 5), and decreased covalency in

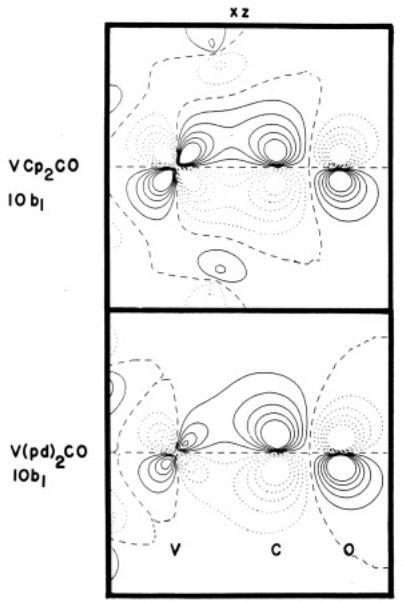

Figure 5. Orbital contour plots in the *xz* plane for the lowest unoccupied $10b_1$ orbitals in Cp_2VCO and pd_2VCO. The contour interval is 0.270 e/Å^3.

Table VIII. Results of Spin-Polarized Calculations for Cp_2VCO

level[a]			% contributns from atoms			
up	down	energy (eV)	V	C	O	C(Cp)
	$9b_2$	−2.20	22	4	1	73
	$14a_1$	−2.22	24	2	1	73
$12b_1$		−2.32	1	12	6	81
	$12b_1$	−2.37	1	11	6	82
$9b_2$		−2.43	14	2	1	83
$14a_1$		−2.43	15	0	1	84
	$7a_2$	−2.53	5	0	0	95
$7a_2$		−2.55	2	0	0	98
	$11b_1$	−3.70	43	19	10	28
	$13a_1$	−3.75	56	20	3	20
	$6a_2$	−3.91	57	0	0	43
	$8b_2$	−4.11	26	31	21	21
$11b_1$		−4.22	27	29	20	22
$8b_2$		−4.23	21	40	27	11
$13a_1$		−4.55	49	22	3	25
$6a_2$		−4.84	52	0	0	48
	$10b_1$	−5.48	12	23	22	41
$10b_1$		−5.72	29	7	10	52
	$12a_1$	−5.78	81	1	0	17
$12a_1$		−6.85	85	1	0	13
	$7b_2$	−7.30	57	19	16	7
$7b_2$		−7.97	71	9	11	8
	$6b_2$	−9.48	1	0	0	98
$6b_2$		−9.55	3	0	0	97
	$11a_1$	−9.68	9	1	0	91
$11a_1$		−9.84	11	0	0	89
	$5a_2$	−9.85	16	0	0	83
	$9b_1$	−10.00	19	1	8	72
$5a_2$		−10.10	25	0	0	75
$9b_1$		−10.25	27	0	9	63

[a] Highest occupied molecular orbital is spin up $12a_1$, and hydrogen contributions (<3%) are not given.

the pd derivative is apparent.

Radical reactivity of Cp_2VCO and pd_2VCO depends critically on the highest occupied $12a_1$ orbital. From the contour plots of Figure 6 we see an interesting difference in the directional properties of this orbital. In Cp_2VCO the electron lies predominantly in the *yz* plane and approximates a d_{y^2} orbital. In pd_2VCO the electron distribution more closely resembles a d_{x^2} orbital. Since a d_{x^2} orbital points toward the η^5-pd ring, it should be shielded

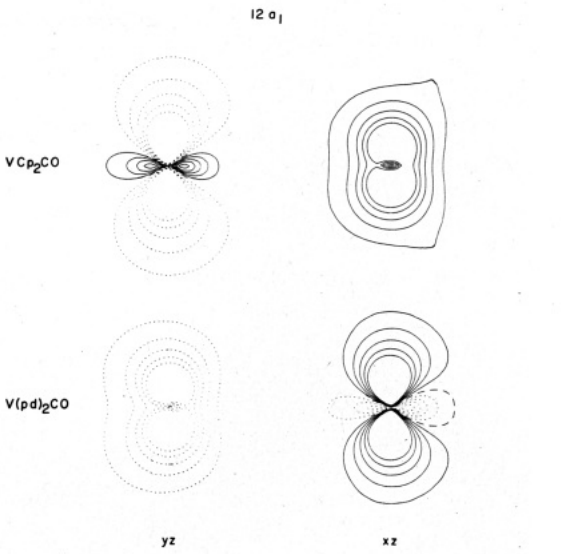

Figure 6. Orbital contour plots in the *yz* and *xz* planes for the highest occupied $12a_1$ orbital of Cp_2VCO and pd_2VCO. Only the vanadium contribution (~80%) to the orbital is shown at contour intervals of 0.270 e/Å^3.

Table IX. Results of Spin-Polarized Calculations for pd_2VCO

level[a]			% contributns from atoms			
up	down	energy (eV)	V	C	O	C(Cp)
	$14a_1$	−2.23	15	0	0	89
$14a_1$		−2.23	9	0	0	94
	$13a_1$	−3.40	51	15	5	27
	$10b_2$	−3.41	39	7	2	51
$10b_2$		−3.94	29	4	2	65
	$8a_2$	−4.02	43	0	0	54
	$11b_1$	−4.13	46	17	7	30
$13a_1$		−4.24	46	17	5	30
$8a_2$		−4.27	5	0	0	94
	$7a_2$	−4.59	27	0	0	70
$11b_1$		−4.83	33	24	13	31
$9b_2$		−5.02	8	38	30	24
	$9b_2$	−5.07	5	33	26	35
$7a_2$		−5.34	46	0	0	49
	$12a_1$	−6.11	80	0	0	14
	$10b_1$	−6.38	4	32	25	36
$10b_1$		−6.38	7	24	19	47
$12a_1$		−7.20	76	1	0	19
	$8b_2$	−8.08	45	9	11	32
	$9b_1$	−8.39	19	2	5	72
$8b_2$		−8.65	58	4	8	26
$9b_1$		−8.68	29	1	4	63
	$11a_1$	−9.34	11	0	0	88
$11a_1$		−9.54	17	1	0	82
	$6a_2$	−10.58	8	0	0	91
$6a_2$		−10.71	12	0	0	86
	$7b_2$	−11.08	0	0	2	98
$7b_2$		−11.08	0	0	2	98
	$8b_1$	−11.13	1	0	0	97
$8b_1$		−11.14	2	0	0	96

[a] Highest occupied molecular orbital is spin up $12a_1$, and hydrogen contributions (<5%) are not given.

from bimolecular attack; however, a d_{y^2} orbital would be more accessible for bimolecular chemical reactions. Experimental support for this difference in hybridization derives from EPR spectroscopic studies (vide infra) and from kinetic studies of reaction rates discussed in a recent paper.[10c] Spin-polarized calculations[19] (Tables VIII and

(19) Slater, J. C. *Quantum Theory of Molecules and Solids. The Self-Consistent Field for Molecules and Solids*; McGraw-Hill: New York; 1974; pp 56–79.

Table X. EPR Parameters for $(\eta^5\text{-L})_2$VCO Complexes[a]

complex	A_{iso} (±0.02)	g_{iso} (±0.002)	T_1 (±0.02)	T_2 (±0.02)	T_3 (±0.02)	g_1 (±0.001)	g_2 (±0.002)	g_3 (±0.003)
pd_2VCO	−7.36	1.991	−12.57	−6.10	−3.39	1.967	1.990	2.005
pd_2'VCO	−7.32	1.991	−12.59	−6.39	−2.97	1.958	1.980	1.999
Cp(pd)VCO	−5.86	1.993	−11.12	−3.95	−2.50	1.975	1.990	2.005
Cp(pd')VCO	−5.76	1.995	−11.02	−3.74	−2.64	1.970	1.984	2.020
Cp_2VCO	−2.68	2.005	−6.98	−2.03	+1.27	1.979	2.039	1.997
Cp^*_2VCO	−1.73	2.004	−5.85	−1.33	+2.15	1.977	2.027	1.997

[a] Hyperfine couplings in units of 10^{-3} cm^{-1}.

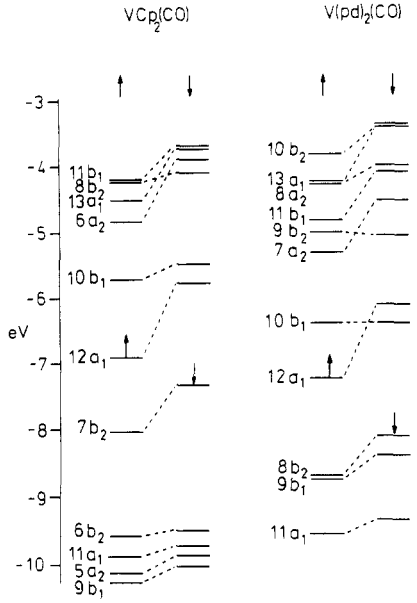

Figure 7. Results of spin-polarized SCF–DV–Xα calculations for Cp_2VCO and pd_2VCO.

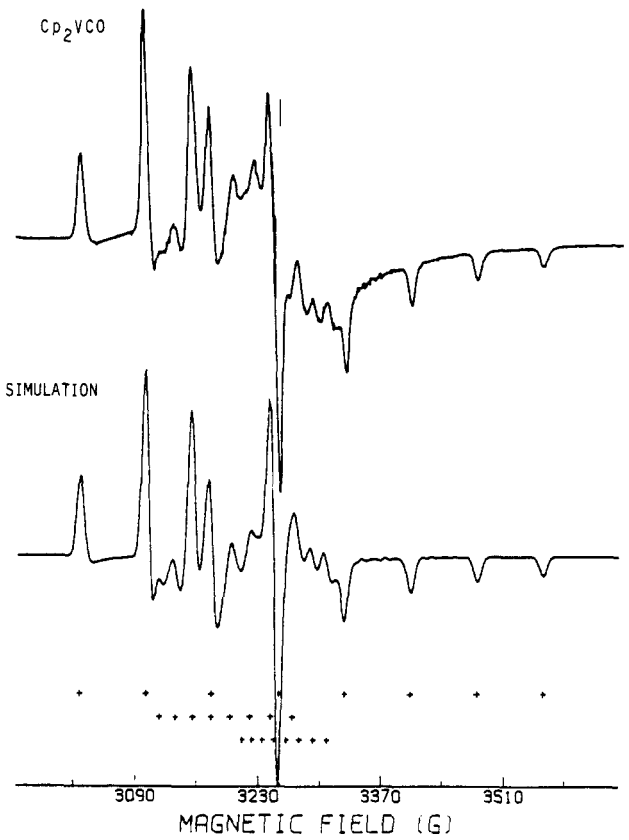

Figure 8. EPR spectrum at 77 K of Cp_2VCO in a frozen methylcyclohexane solution (frequency 9.116 GHz). A computer simulation is shown below the experimental spectrum. The value of g_e is shown by the vertical dash in this and the following figures.

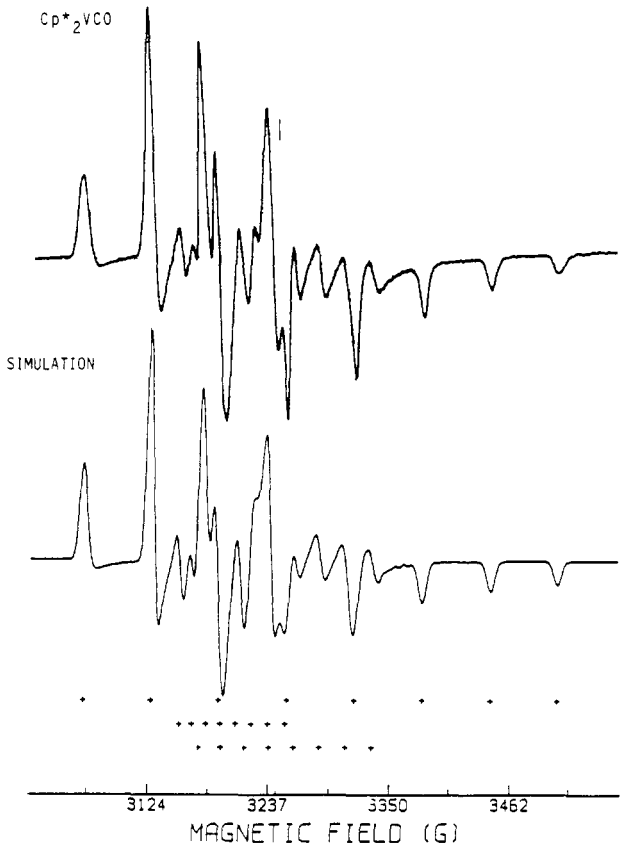

Figure 9. EPR spectrum at 77 K of Cp^*_2VCO in a frozen methylcyclohexane solution (frequency 9.092 GHz). A computer simulation is shown below the experimental spectrum.

IX and Figure 7) support the conclusions derived from the spin-restricted studies and provide information used in the ensuing discussion of EPR spectra.

EPR Spectroscopic Studies. The EPR spectra of pd_2VCO, pd'_2VCO, Cp(pd)VCO, Cp(pd')VCO, Cp_2VCO, and Cp^*_2VCO in methylcyclohexane solvent all show an eight-line signal from the interaction of an unpaired electron with one ^{51}V ($I = {}^7/_2$) nucleus. Isotropic g and A values for the complexes are listed in Table X. In frozen solution at 77 K, spectra that consist of three overlapping eight-line signals (Figures 8–13) are observed. The three components of the **T** and **g** tensors can be estimated from the spectra, and best values of these parameters (Table X) are obtained from computer simulations (Figures 8–13) that use an effective spin Hamiltonian and assume coincidence of the **g** and **T** (hyperfine) tensors. This assumption appears valid, since the simulated spectra accurately reproduce peak positions and relative intensities. The assumed coincidence of the tensor axes has been proven in similar systems of high molecular symmetry.[20] Resulting values of the three components of the **T** and **g**

(20) Petersen, J. L.; Dahl, L. F. *J. Am. Chem. Soc.* **1975**, *97*, 6422–6433.

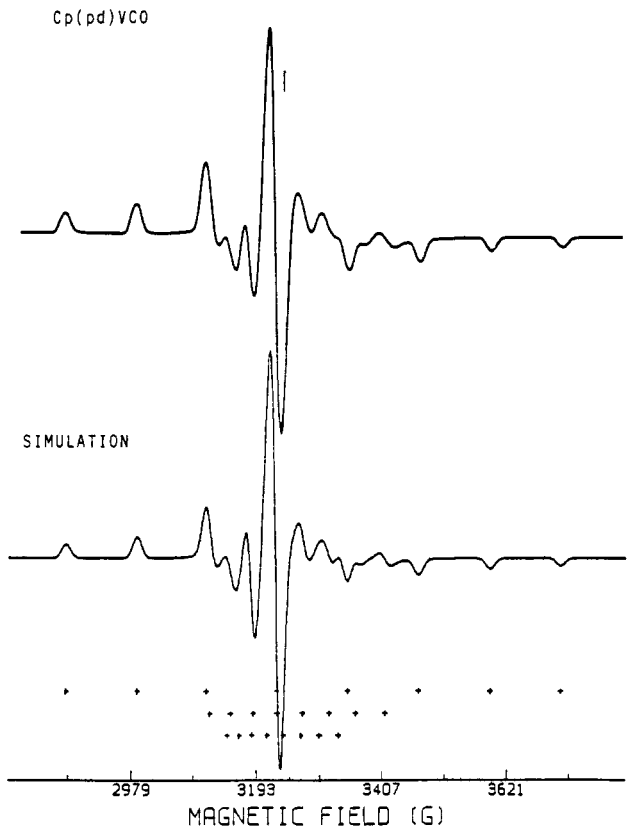

Figure 10. EPR spectrum at 77 K of Cp(pd)VCO in a frozen methylcyclohexane solution (frequency 9.099 GHz). A computer simulation is shown below the experimental spectrum.

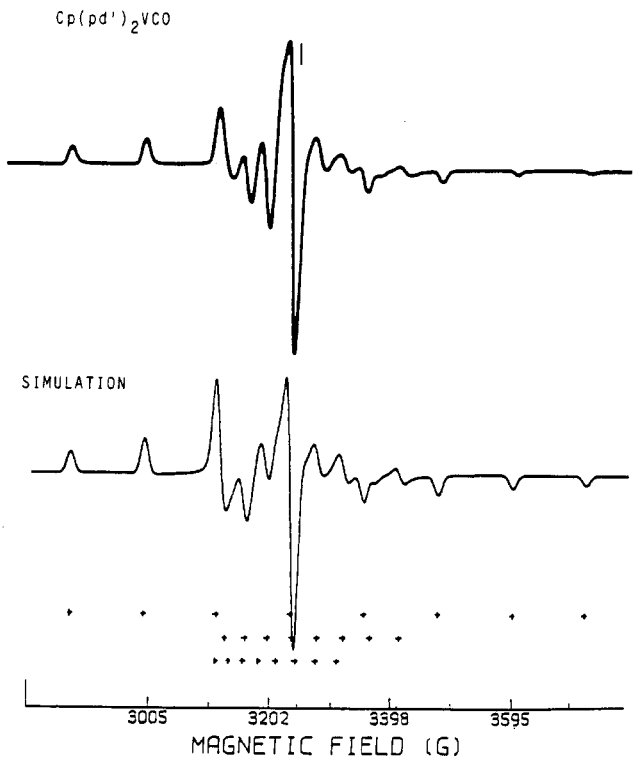

Figure 11. EPR spectrum at 77 K of Cp(pd')VCO in a frozen methylcyclohexane solution (frequency 9.091 GHz). A computer simulation is shown below the experimental spectrum.

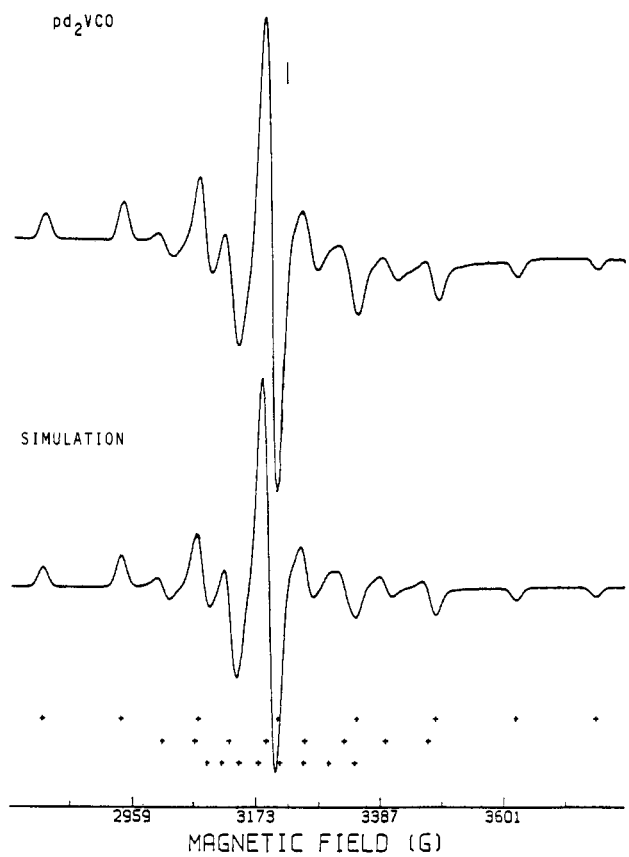

Figure 12. EPR spectrum at 77 K of pd_2VCO in a frozen methylcyclohexane solution (frequency 9.040 GHz). A computer simulation is shown below the experimental spectrum.

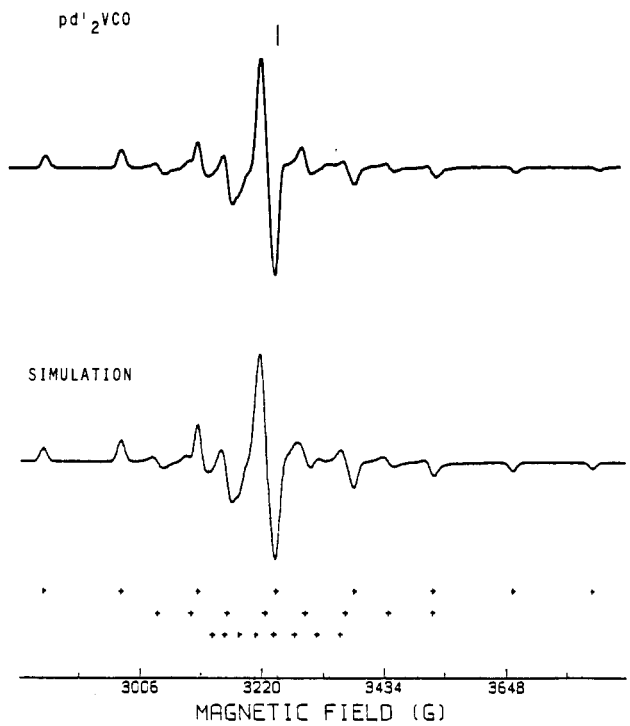

Figure 13. EPR spectrum at 77 K of pd'_2VCO in a frozen methylcyclohexane solution (frequency 9.096 GHz). A computer simulation is shown below the experimental spectrum.

tensors are given in Table X. The anisotropy in the hyperfine components suggests more than one d orbital contributes to the electronic ground state. In a C_{2v} structure mixing of the d orbitals is allowed only for the a_1 representation, which contains the d_{z^2}, $d_{x^2-y^2}$, p_z, and s orbitals of the metal. An A_1 ground state, in which the unpaired electron resides in an orbital of large a_1 d character, is predicted by the MO calculations discussed above. The validity of this choice has been demonstrated for several Cp_2VL_2 complexes.[20-29]

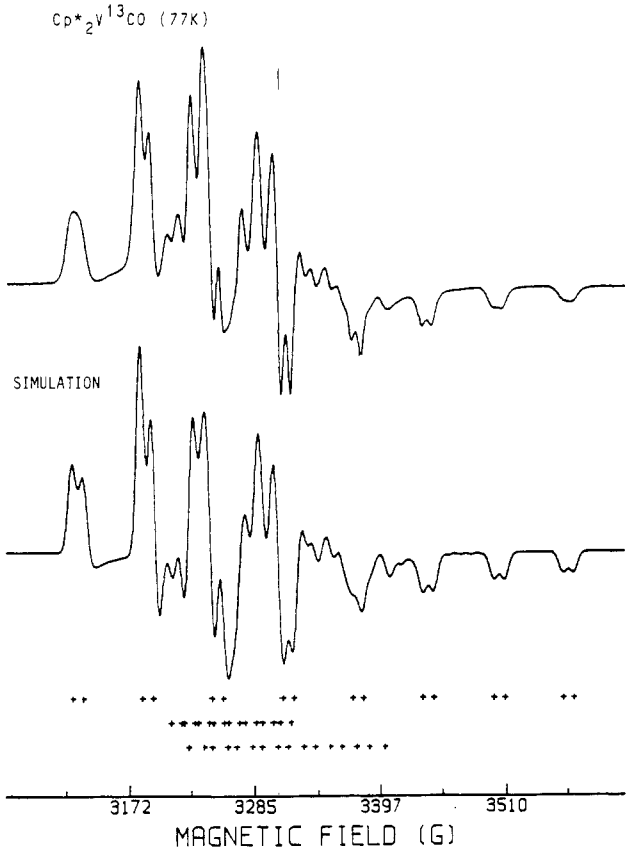

Figure 14. EPR spectrum of $Cp^*_2V^{13}CO$ in a frozen methylcyclohexane solution at 77 K (frequency 9.261 GHz) along with the simulated spectrum.

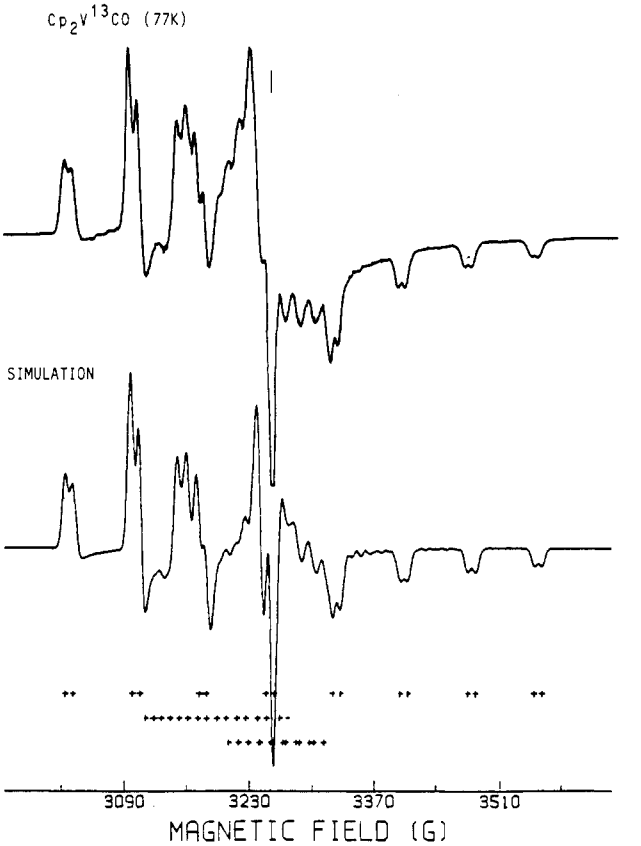

Figure 15. EPR spectrum of $Cp_2V^{13}CO$ in a frozen methylcyclohexane solution at 77 K along (frequency 9.116 GHz) with the simulated spectrum.

Table XI. Superhyperfine Parameters for $Cp_2^*V^{13}CO$ and $Cp_2V^{13}CO$

	$Cp^*_2V^{13}CO$	$Cp_2V^{13}CO$
A^C_{iso} cm^{-1} ($\pm 0.2 \times 10^{-4}$)	10.7×10^{-4}	9.3×10^{-4}
A_1, cm^{-1} ($\pm 0.3 \times 10^{-4}$)	8.8×10^{-4}	8.0×10^{-4}
A_2, cm^{-1} ($\pm 0.3 \times 10^{-4}$)	9.0×10^{-4}	9.3×10^{-4}
A_3, cm^{-1} ($\pm 0.1 \times 10^{-4}$)	13.0×10^{-4}	10.6×10^{-4}
B,[a] cm^{-1}	1.4×10^{-4}	0.7×10^{-4}
% C(4s)	0.85	0.74
% C(4p)	3.8	2

[a] $B = (A_\parallel - A_\perp)/3$, where $A_\parallel = A_3$ and $A_\perp = (A_1 + A_2)/2$.

A negative sign for most of the hyperfine components in Table X is assumed by analogy to similar vanadium complexes, where an unpaired spin in a d orbital leads to negative values of T. The average of T_1, T_2, and T_3 for all pentadienyl complexes nearly equals A_{iso}, therefore, all four coupling constants have the same sign. For Cp_2VCO and Cp^*_2VCO, the average of the hyperfine components does not equal A_{iso} unless the sign of T_3 differs from that of T_1, T_2, and A_{iso}.

The EPR spectra of the ^{13}CO-labeled complexes were examined to probe the extent of spin delocalization onto the carbonyl ligands. No ^{13}C superhyperfine interaction is observed in the ambient or liquid-nitrogen-temperature spectra of $pd_2V^{13}CO$ or $Cp(pd)V^{13}CO$. For $Cp^*_2V^{13}CO$, an isotropic ^{13}CO splitting of 11.4 G (10.7×10^{-4} cm^{-1}) is observed in the solution spectrum, and an anisotropic splitting of $A_\parallel = 13.0 \times 10^{-4}$ and $A_\perp = 8.9 \times 10^{-4}$ cm^{-1} is observed in the frozen solution spectrum (Figure 14 and Table XI). For $Cp_2V^{13}CO$, a ^{13}C superhyperfine interaction of smaller magnitude (Figure 15 and Table XI) is found. A comparison of isotropic and anisotropic ^{13}C hyperfine components allow an estimate of the spin population in the carbon s and p orbitals. For Cp^*_2VCO, the s character determined from the isotropic value ($A^C_{iso} = 10.7 \times 10^{-4}$ cm^{-1}) and the calculated isotropic value[30] for a carbon s electron of 3777 MHz (0.126 cm^{-1}) yields $10.7 \times 10^{-4}/0.126 = 0.0085$ fractional s character. Similarly, the p orbital population, estimated by comparing the observed anisotropic contribution, $^1/_3$ of $(A_\parallel - A_\perp)$, to the calculated value[30] (3.583×10^{-3} cm^{-1}) for a carbon 2p electron, gives $^1/_3$ $(13.0\text{–}8.9) \times 10^{-4}/3.583 \times 10^{-3} = 0.038$ p character. An s to p ratio of 1:4.4 suggests that the delocalization of the unpaired spin on the carbonyl group occurs via the CO π^* orbitals, which (Figure 4 and 5) contain a large amount of carbon p character. A similar calculation for Cp_2VCO gives a carbon 2s contribution of 0.0074 and a p contribution of 0.019 (using $(A_1 + A_2)/2$ for $A_\perp$). The sum of the s and p contributions accounts for 4.6% of the unpaired spin density in Cp^*_2VCO and 2.7% in Cp_2VCO. The calculated spin distribution (Table V) overestimates by 2–3 the small amount of unpaired spin

(21) Brintzinger, H. H.; Lohr, L. L., Jr.; Tang Wong, K. L. *J. Am. Chem. Soc.* **1975**, *97*, 5146–5155.
(22) Green, J. C.; Jackson, S. E.; Higginson, B. *J. Chem. Soc., Dalton Trans.* **1975**, 403–409.
(23) Lauher, J. W.; Hoffmann, R. *J. Am. Chem. Soc.* **1976**, *98*, 1729–1742.
(24) Bakalik, D. P.; Hayes, R. G. *Inorg. Chem.* **1972**, *11*, 1734–1738.
(25) Stewart, C. P.; Porte, A. L. *J. Chem. Soc., Dalton Trans.* **1973**, 722–729.
(26) Petersen, J. L.; Lichtenberger, D. L.; Fenske, R. F.; Dahl, L. F. *J. Am. Chem. Soc.* **1975**, *97*, 6433–6441.
(27) Petersen, J. L.; Dahl, L. F. *J. Am. Chem. Soc.* **1975**, *97*, 6416–6422.
(28) Evans, A. G.; Evans, J. C.; Espley, D. J. C.; Morgan, P. H.; Mortimer, J. *J. Chem. Soc., Dalton Trans.* **1978**, 57–61.
(29) Casey, A. T.; Raynor, J. B. *J. Chem. Soc., Dalton Trans.* **1983**, 2057–2062.
(30) Morton, J. R.; Preston, K. F. *J. Magn. Reson.* **1978**, *30*, 577–582.

Table XII. Calculated Parameters and Orbital Contributions to the SOMO in $(\eta^5\text{-L})_2$VCO Complexes

complex	P (10^{-4} cm^{-1})	κ (10^{-4} cm^{-1})	χ (au)	% d	% 4s (V)	% CO	ν(CO), cm^{-1}
pd_2VCO	91.3	72.2	−2.31	71.3	1.14	*a*	1959
pd_2'VCO	94.1	71.0	−2.27	73.5	1.23	*a*	1944
Cp(pd)VCO	90.2	57.5	−1.84	70.5	2.20	*a*	1938
Cp(pd')VCO	87.3	57.0	−1.82	68.2	2.23	*a*	1935
Cp_2VCO	82.9	26.0	−0.834	64.8	4.47	2.7	1881
Cp^*_2VCO	80.0	16.6	−0.532	62.5	5.15	4.7	1842

[a] Estimated less than 1.5%.

density on the carbonyl ligands; however, the trend (greater spin density on the CO ligand in the Cp complex) is correct.

With use of the equations presented by McGarvey,[31] the relative d_{z^2} and $d_{x^2-y^2}$ contributions to the SOMO can be determined from the anisotropy of the **g** and **T** components. This analysis has been used to determine the orientation and shape of the SOMO for other Cp_2VX_2 complexes. Unfortunately, in the absence of single-crystal data, an unambiguous assignment of the tensor components in Table X to the molecular axes is not possible (vide infra).

The values of the isotropic coupling constant (κ) and the hyperfine parameter (P) obtained from this analysis are independent of the assignment of the hyperfine components to the molecular axes and allow a more meaningful comparison of these complexes. The hyperfine parameter of P reflects the effective charge on vanadium (eq 1).

$$P = g_e g_n(^{51}\beta)\beta_n\langle r^{-3}\rangle \quad (1)$$

Values of this parameter are given in Table XII. The low values of P for these complexes correspond to effective charges on vanadium of 0 to +1. The P value of 8.29×10^{-3} cm^{-1} for Cp_2VCO may be compared to that for a d electron in a V^{2+} ion,[32] $P = 12.8 \times 10^{-3}$ cm^{-1}. The ratio $P/P_{V(II)}$ (= 0.648 for Cp_2VCO) shows that 65% of the unpaired spin density resides in the vanadium d orbitals. Replacement of a cyclopentadienyl ligand with pentadienyl leads to a greater positive charge on vanadium and decreased delocalization of the d electrons from the metal center; the calculated % d character of the SOMO in Table XII illustrates this trend.

The isotropic contribution to the coupling (or contact term), κ, nearly equals A_{iso}, since g_{iso} approximates the free electron value (eq 2).

$$A_{iso} = -\kappa + (g_{iso} - g_e)P \quad (2)$$

The contact term κ may be used to determine χ (eq 3), where χ reflects the polarization of the inner s electrons through an exchange reaction with the unpaired electron.[32]

$$\kappa = -(^2/_3)g_e g_n(^{51}\beta)\beta_n\chi \quad (3)$$

Values of χ less negative than −2.82 au arise from direct mixing of the 4s orbital into the ground state. After correcting for exchange polarization of the 1s, 2s, and 3s elecrons, which contributes -8.81×10^{-3} cm^{-1} (for a V^{2+} ion) to the isotropic term,[33] the 4s contribution is calculated (eq 4). The value of a_{4s} for Cp_2VCO (= -2.60×10^{-3} + 8.81×10^{-3} cm^{-1}) can then be compared with the calculated value of 4165 MHz (0.1389 cm^{-1}) for an electron in a vanadium 4s orbital.[30] The calculated spin population in the 4s orbital is 0.0447 (= $6.21 \times 10^{-3}/0.1389$), or 4.5% of the unpaired spin density. Similar calculations yield smaller 4s contributions for the pentadienyl complexes (Table XII). Slight differences in the 4s populations have a larger effect on the magnitude of the components of the **T** tensor; the increasing (positive) 4s contribution in the series of complexes in Table X accounts for the trend toward decreasing A_{iso}, and in Cp_2VCO and Cp^*_2VCO this effect is large enough to cancel the negative polarization term for T_3. The increased 4s contribution agrees with the greater covalency suggested by the lower values of P.

$$-\kappa = a_{4s} + a_{1,2,3s} \quad (4)$$

The sum of the calculated vanadium 4s and 3d contributions to the SOMO account for 70–75% of the unpaired spin density in these complexes (Table XII). For the bis(cyclopentadienyl) complexes, delocalization of the spin onto the CO ligand may account for another 2–5%. The remaining spin density may be delocalized over the other ligands or among other metal orbitals (for instance, the p_z orbital can also mix into the A_1 ground state, a contribution which is difficult to estimate, and deviations from the assumed C_{2v} symmetry could allow contributions from other metal orbitals.) Results of the spin-polarized calculations (Table V) confirm that most spin density occurs in the V 3d and 4s orbitals and that the 3d + 4s spin density in the pentadienyl complexes slightly exceeds that in the cyclopentadienyl complexes.

Attempts to calculate relative d_{z^2} and $d_{x^2-y^2}$ contributions to the SOMO in the manner used for several other 17-electron Cp_2VX_2 is complicated by a variety of factors, the most important of which is the uncertainty in assigning the components of the **T** and **g** tensors to the molecular axes. Assignment of the least negative hyperfine component T_3 to T_z seems reasonable based on analogy with Cp_2VX_2 complexes[20,27] and theoretical calculations,[21,34,35] which indicate the SOMO is largely d_{y^2} in character. However, assignment of the other two T components to the x or y axes is less certain. Even if T_1 and T_2 could be assigned "correctly" for the cyclopentadienyl complexes, the analogous assignment is not necessarily the correct choice for the pentadienyl complexes. The assignment of T_3 as T_z is also questionable in view of the results for the ^{13}CO-labeled complexes: in the EPR spectra of $Cp_2V^{13}CO$ and $Cp^*_2V^{13}CO$, the unique ^{13}C component $A^C_{\parallel}$ is associated with the T_3^V and would seem to indicate T_3 is directed along the V–CO (z) axis. In the SOMO, which results from this assignment, the majority of the unpaired spin would be localized along this axis. This description differs substantially from the orbital description for Cp_2VX_2 complexes and that predicted by the SCF–Xα–DV calculations and seems even less reasonable for the pentadienyl complexes, for which no ^{13}C coupling was observed.

Regardless of the assignment, the relative $d_{x^2-y^2}$ and d_{z^2} orbital contributions calculated by these methods for the mixed cyclopentadienyl–pentadienyl complexes are not

(31) McGarvey, B. R. In *Electron Spin Resonance of Metal Complexes*; Yen, T. F., Ed.; Plenum: New York, 1969.
(32) McGarvey, B. R. *J. Phys. Chem.* **1967**, *71*, 51–67.
(33) Robertson, R. E.; McConnell, H. M. *J. Phys. Chem.* **1960**, *64*, 70–77.
(34) Lauher, J. W.; Hoffmann, R. *J. Am. Chem. Soc.* **1976**, *98*, 1729–1742.
(35) Green, J. C.; Jackson, S. E.; Higginson, B. *J. Chem. Soc., Dalton Trans.* **1974**, 403–409.

intermediate between those of the bis(cyclopentadienyl) or bis(pentadienyl) complexes. The covalent bonding in these complexes and deviations from C_{2v} symmetry could allow mixing of other orbitals into the ground state, which were not considered in this analysis. The coincidence of the vanadium (and ^{13}C) **T** and **g** tensors has also been assumed, and the combination of these uncertainties prohibit a definitive comparison of the orientation of the SOMO in this series of complexes.

Spin–orbit coupling arising from the mixing of excited states with the ground-state wave function may also be significant in these complexes and is reflected in the deviations of the components of the **g** tensor from the free electron value. In particular, the values of g_{iso} and g_3 for Cp_2VCO and Cp^*_2VCO, which are greater than the free electron value, suggest spin–orbit coupling occurs between the a_1 orbital and an occupied d_{xy}, d_{xz}, or d_{yz} orbital, depending on the assignment of g_3. The orbital energy diagram for Cp_2VCO (Figure 7) suggests that this orbital ($7b_2$) is largely d_{yz} in character and is involved in π-bonding with the CO ligand. The significance of this interaction is uncertain but is consistent with the enhanced V–CO π interactions illustrated by the low carbonyl stretching frequencies (Table XII) and the observable ^{13}C hyperfine splitting in the bis(cyclopentadienyl) complexes. The g values that are less than g_e indicate coupling between the ground state and an unoccupied orbital. Given the uncertainties in the orientation of the **g** tensor in these complexes, a detailed discussion is unwarranted.

Conclusions

The EPR results and the SCF–Xα–DV calculations both argue for less ionicity and greater covalency in the ring–V bonding in Cp_2VCO than in pd_2VCO. Both analyses indicate a lower positive charge on vanadium for the cyclopentadienyl complexes, and the EPR results show that this charge increases as the electron-withdrawing ability of the η^5-ligand increases. Vanadium–carbonyl π-bonding is also enhanced as the electron-donating ability of the η^5-ligand increases, as indicated by the observed hyperfine interactions between the unpaired electron and the CO ligand in $Cp_2V^{13}CO$ and $Cp^*_2V^{13}CO$ and the trend toward decreasing carbonyl stretching frequencies as pentadienyl ligands are replaced with cyclopentadienyl ligands. Electron density maps from the SCF–Xα–DV calculations predict that the SOMO for pd_2VCO resembles a d_{x^2} orbital, while the Cp_2VCO SOMO is more nearly d_{y^2} in character.

Differences in the electronic structures of these complexes may be responsible for the very different reactivities of these complexes, which are difficult to rationalize by steric arguments alone. Ligand exchange and substitution reactions for Cp_2VCO and Cp^*_2VCO occur by a rapid associative pathway, whereas the pentadienyl complexes are relatively inert and undergo substitution by a much slower dissociative pathway.[10] Substitution of a single pd for a Cp ligand, as in Cp(pd)VCO, suffices to quench the associative reaction path. The electronic parameters (Table XII), which describe the distribution of the odd electron, as well as the values of ν_{CO}, show a similar discontinuity as a single pd ligand replaces a Cp ligand. The increased covalency and delocalization of the unpaired electron should facilitate associative reactions for the cyclopentadienyl complexes if nucleophilic attack occurs via the half-occupied a_1 orbital.[10c] The different substitution labilities of the pentadienyl and cyclopentadienyl complexes may also be related to the different orientations of the SOMO; in pd_2VCO, the SCF–Xα–DV calculations predict that the SOMO is partially shielded by the pentadienyl ligands and would be less accessible to attack by an incoming nucleophile than in Cp_2VCO.

Acknowledgment. This material is based on work supported by the National Science Foundation (CHE-8504088 to W.C.T. and CHE-8514366 to F.B.). We thank Professors R. N. Perutz, B. M. Hoffman, and R. D. Ernst for helpful discussions.

Registry No. pd_2VCO, 103905-30-2; $(2,4\text{-}Me_2\text{-}pd)_2VCO$, 86994-95-8; Cp(pd)VCO, 103905-31-3; Cp(pd′)VCO, 103905-32-4; Cp_2VCO, 53339-41-6; Cp^*_2VCO, 83260-22-4; $Cp^*_2V^{13}CO$, 109283-50-3; $Cp_2V^{13}CO$, 109283-49-0; Cp_2V, 1277-47-0; pd_2V, 113860-31-4.